Wiebold Wurpts, Jens Twiefel* and Francois Brouet

Equivalent Circuit Parametrization Utilizing FE Model Order Reduction and its Application to Piezoelectric Generators and Actuators

https://doi.org/10.1515/ehs-2017-0002

Abstract: Equivalent circuits are often the first choice for the modeling of piezoelectric systems, as they allow for the consideration of the complete electro-mechanical system with one or even more modes. The parameters of the equivalent circuit model are identified by a measured or simulated frequency response. In this contribution a method for a direct modal condensation of the equivalent parameters for arbitrary FE structures and loads is described and discussed. First the proposed method is demonstrated for a continuous piezoelectric rod and then applied to discrete finite element models. The derived equivalent circuit has an identical appearance to the classical solution, but additionally allows arbitrarily load conditions. Furthermore, the structure of the derived equivalent circuit depends on whether short- or open-circuited modes are used for the modal expansion. The influence of truncated modes is discussed utilizing residual terms, leading to a better understanding of the circuit parameters. Additionally the model based approaches in the third part an experimental parameter identification procedure for many modes is presented as well. The influence of the load and the quality of the model order reduction are discussed for piezoelectric rods. The methods are demonstrated for a base excited energy harvesting system an ultrasonic grubber.

Keywords: equivalent circuits, model order reduction, piezoelectric systems

Introduction

The modeling of technical systems with multiple physical domains is often quite challenging. With equivalent circuits (EQCs) different physical domains are mapped into the electrical domain, which gives a unified description of multiphysical problems. Especially the electrical input behavior of piezoelectric resonators is identical to the input behavior of certain electrical networks. The classical Butterworth- Van Dyke EQC was proposed in the early 1930s (Dyke, 1928) and is still widely used to model resonant piezoelectric systems (e.g. Wurpts and Twiefel 2013). It consists of a capacitance and parallel serial LCR resonators, each representing one mechanical mode. Mason (1942) derived the circuit from the analytical solution of a one dimensional piezoelectric rod. He established the exact relation between the mechanical properties of an one dimensional rod and the EQC. In this way concentrated forces are considered, but as the mechanical load or the geometry of the system becomes more complex, an analytical solution is not possible anymore and this approach is limited. Therefore the EQCs of technical systems are most often identified by an experimental frequency response as described by (Richter et al. 2009).

In linear elasticity the forced response of a body is expanded into a modal series. This approach is applied by (Tiersten 1969) in the 1970s to piezoelectric continua. The electric input admittance of a three dimensional linear piezoelectric continuum is presented by (Holland and EerNisse 1968). They discretize the continuum with elastic eigenmodes and derive a condensed model of the piezoelectric system. Hagood et al. Hagood et al. (1990) use a general assumed mode approach within the variational formulation. A broad overview on the modal expansion and the related EQCs especially for different physical domains is also due to (Tilmans 1997).

Nowadays technical systems are most often modeled using the finite element approach. With increasing complexity an efficient model order reduction as proposed by Becker et al. (Becker et al. 2006) becomes relevant. The modeling of different physical domains is possible within the concept of substructuring, as proposed by (Collet and Cunefare 2008). Both approaches can effectively calculate piezoelectric structures with arbitrary loadings, but the relation to the widely known and trusted EQCs is not clear. Elvin and Elvin (2009) present a modal reduction

***Corresponding author: Jens Twiefel,** Institute of Dynamics and Vibration Research, Leibniz Universität Hannover, Appelstr. 11, Hannover 30159, Germany, E-mail: twiefel@ids.uni-hannover.de

Wiebold Wurpts, Netzsch Gabo Instruments GmbH, Ahlden, Germany

Francois Brouet, Herrmann Ultraschall GmbH, Karlsbad, Germany

of a discrete piezoelectric model as well as the corresponding EQC. This approach is generalized and applied to FE-models within this paper.

In the first section the proposed reduction is applied to the well known piezoelectric rod. Even if the obtained EQC is apears to be identical to the classical derivation by (Mason 1942) it now allows arbitrary loads. Furthermore the different classical circuits with and without a negative capacitance are a result of different modal expansions, using the short- or the open-circuited modes respectively. This section gives a theoretical foundation of the method, but may be skipped if the reader is more interested in the FE-reduction. In the second section the reduction of discrete FE-models is discussed and in the third section an experimental identification procedure for many modes is presented. The fourth section consists of four examples, that also contain further aspects.

Piezoelectric Rod

Many piezoelectric systems are sufficiently described by waves propagating in only one dimension. The piezoelectric rod is thereby the simplest continuous model for a piezoelectric resonator. According to Gauss's law the electrical displacement field in every insulating material obeys div $\mathbf{D} = 0$. Although this is true in every piezoelectric material, this is not always the best description of a technical system. If the electrodes of a thin piezoelectric layer are parallel to the direction of wave propagation, a one dimensional approach will cause the electrical field to be constant $E' = 0$. This situation occurs, for example, in piezoelectric bimorphs or plates. Ikeda (1996) formulates more generally, that the direction of polarization and wave propagation are orthogonal and calls this a T-effect (thickness) vibration. On the other hand a piezoelectric ceramic, that is driven in longitudinal direction may be said to cause L-effect (longitudinal) vibration, as the directions of polarization and wave propagation are identical. In the following the EQCs will be derived for L-effect coupling, but an analog treatment of the T-effect should be possible. Because the electric displacement D is constant over the length, it is convenient to use the strain S and D as independent variables.

The equations of motion for the coupled problem are derived using Hamiltons principle. The variational formulation also offers the elegant discretization of the problem. Hamiltons principle

$$\delta \int_{t_0}^{t_1} L + W \quad \mathrm{d}t = 0 \tag{1}$$

states, that the time integral of the Lagrangian $L = E_{\mathrm{kin}} - U$ and the work performed by external forces W becomes extremal between two arbitrary points of time. In the specific inner energy $U^* = TS + ED$ the strain S and D are the independent variables. All values here and in the following are indicated in the direction of polarization. The constitutive equations of linear piezoelectricity in (S,D)-form

$$T = c^{\mathrm{D}} S - hD \tag{2}$$

$$E = -hS + \beta^{\mathrm{S}} D \tag{3}$$

define the stress T and the electrical field E as functions of S and D. In most datasheets the constants h and β^{S} are not given explicitly, but they obey the relations $\beta^{\mathrm{S}} = 1/\varepsilon^{\mathrm{S}}$ and $h \approx e/\varepsilon^{\mathrm{S}}$. The variation of the inner energy of a rod with cross-section A and length l is

$$\begin{aligned} \delta U &= A \int_{-l/2}^{l/2} \delta U^* \mathrm{d}z \\ &= A \int_{-l/2}^{l/2} \delta w' (c^{\mathrm{D}} w' - hD) + \delta D(-hw' + \beta^{\mathrm{S}} D)\ \mathrm{d}z. \end{aligned} \tag{4}$$

The variation of the work W performed by external point forces F_i, a force density F_{V} and applied voltage V is

$$\delta W = \sum_{\mathrm{i}} F_i \delta w_i + V \delta Q + \int_{-l/2}^{l/2} A F_{\mathrm{V}} \delta w \ \mathrm{d}z. \tag{5}$$

Here δw_i is the variation of displacement at the force application point and $Q = DA$ is the charge. In order to obtain the isochronal eigenvibrations of the rod, the conservative system with $W = 0$ is considered first. After integration by parts of δU, the variation of the kinetic energy and with the condition $D' = 0$ the equation of motion for the undamped eigenproblem follow as

$$-\rho \ddot{w} + c^{\mathrm{D}} w'' = 0. \tag{6}$$

The possible boundary conditions also follow directly from the variations as

$$\begin{aligned} \delta w(\pm l/2) = 0 \text{ or } c^{\mathrm{D}} w'(\pm l/2) - hD = 0 \\ \delta D \text{ or } l\beta^{\mathrm{S}} D - hw(l/s) + hw(-l/2) = 0. \end{aligned} \tag{7}$$

The boundary conditions can be interpreted as constant displacement or zero stress and constant electrical displacement or zero voltage. It is remarkable that in the (S,D)-formulation only one partial differential equation is necessary, while in the (S,E)-formulation two coupled equations are needed. With the harmonic ansatz

$w(z,t) = W(z)\exp(j\Omega t)$ the partial differential equation is transformed into a boundary value problem

$$w'' + \lambda^2 w = 0 \quad , \quad \lambda^2 = \frac{\rho\Omega^2}{c^D} \tag{8}$$

with the same boundary conditions eq. 7.
The solution of the eigenvalue problem is discussed in detail by Cady (1946). Here only the results for mechanical force free boundary conditions are given. Cosine-eigenmodes have the same displacement at both sides of the rod and are not excited by an external voltage. Therefore only the sine modeshapes

$$W_i(z) = a_i \sin(\lambda_i z) \tag{9}$$

with the arbitrary scaling factors a_i contribute to the electrical behaviour. The eigenfrequencies follow as $\omega_i = c_0\lambda_i$ with the wave velocity $c_0 = \sqrt{c^D/\rho}$. Zero voltage or short-circuited electrodes correspond with the resonance and lead to a transcendental equation

$$\frac{\tan b_i}{b_i} = \frac{\beta^S c^D}{h^2} \quad \text{with} \quad b_i = \frac{\lambda_i l}{2} \tag{10}$$

for the possible wavenumbers λ_i. On the other hand zero current or open-circuited electrodes correspond with the antiresonance and the possible wavenumbers follow analytically as

$$\lambda_i = \frac{(2i-1)\pi}{l}. \tag{11}$$

It is interesting to note, that with isolated electrodes the classical half-wavelength mode is performed, while with short-circuited electrodes the strain is not zero at the boundaries. Due to the electrical displacement the stress vanishes at the boundaries in any case.
The variational formulation by eq. 1 is the starting point for the discretization of the piezoelectric rod. Following the same patterns as Holland and EerNisse (1968) the harmonic displacements and strains are expanded into a Ritz-ansatz with the eigenfunctions $W_i(z)$, the corresponding strains $W_i'(z)$

$$W(z) = \sum_{i=1}^{n} W_i(z) q_i = \mathbf{W}^T\mathbf{q} \tag{12}$$

$$W'(z) = \sum_{i=1}^{n} W_i'(z) q_i = \mathbf{W'}^T\mathbf{q} \tag{13}$$

and the modal amplitudes $\mathbf{q}$. For the following calculations the sums are written in matrix notation, as is also usual for finite element derivations (Allik and Hughes 1970). The variations of the ansatz simply follow as $\delta\mathbf{W} = \mathbf{W}^T\delta\mathbf{q}$ and $\delta\mathbf{W}' = \mathbf{W'}^T\delta\mathbf{q}$. The ansatz for the electric displacement D differs, whether zero voltage or zero current modeshapes are used. Due to the completely analytical expressions, the case of zero current modeshapes is discussed first.

Discretization with Open-Circuited Modeshapes

In this case the modeshapes do not contribute to the electrical displacement and therefore the piezo-charge Q still is an independent variable. With Gauss's law the electric displacement and its variation are

$$D = Q/A \quad \text{and} \quad \delta D = \delta Q/A. \tag{14}$$

The ansatz functions are inserted into the energy and work variations (Equation 4 and 5) and then grouped into mechanical and electrical degrees of freedom. The variation of the kinetic and inner energy leads to the mass and stiffness matrices

$$\mathbf{M}_{qq} = A\rho \int_{-l/2}^{l/2} \mathbf{W}\mathbf{W}^T \, dz = \mathbf{diag}(m_{ii}) \tag{15}$$

$$\mathbf{K}_{qq} = Ac^D \int_{-l/2}^{l/2} \mathbf{W}'\mathbf{W}'^T \, dz = \mathbf{diag}(k_{ii}) \tag{16}$$

$$\mathbf{K}_{qe} = \mathbf{K}_{eq}^T = -h \int_{-l/2}^{l/2} \mathbf{W}' dz = \int_{-l/2}^{l/2} \mathbf{E} dz = \mathbf{V}_R \tag{17}$$

$$K_{ee} = \frac{1}{C_0} \quad \text{with } C_0 = \frac{A}{l\beta^S}. \tag{18}$$

The modeshapes are orthogonal as shown in the appendix, but each modeshape W_i induces an electrical voltage V_{Ri}. The sign of the reaction voltage depends on the scaling of the modeshape. Voltage and charge are directly coupled with the dielectric capacity C_0. It should be noted, that the capacity C_0 does not consider any piezoelectric coupling and hence is identical to the total capacitance for zero strain.
The ansatz functions are also inserted into the work W leading to the modal forces

$$\mathbf{F}_q = \sum_i \mathbf{F_i}\mathbf{W}_I + A \int_{-\mathbf{l/2}}^{\mathbf{l/2}} \mathbf{F}_V \mathbf{W}(z) \, dz, \tag{19}$$

where $\mathbf{W}_I$ is the vector of modal displacements at the point of force application. The resulting matrices are grouped to

form the complete electro-mechanical model

$$\begin{bmatrix} \mathbf{M_q} & \mathbf{0} \\ \mathbf{0} & 0 \end{bmatrix} \begin{pmatrix} \ddot{\mathbf{q}} \\ \ddot{Q} \end{pmatrix} + \begin{bmatrix} \mathbf{K}_{\mathrm{qq}} & \mathbf{V}_{\mathrm{R}} \\ \mathbf{V}_{\mathrm{R}}^{\mathrm{T}} & 1/C_0 \end{bmatrix} \begin{pmatrix} \mathbf{q} \\ \mathrm{Q} \end{pmatrix} = \begin{pmatrix} \mathbf{F}_{\mathrm{q}} \\ V \end{pmatrix}. \tag{20}$$

The harmonic response of the condensated model is investigated for a voltage excitation $V(t) = \mathrm{Re}\{\hat{V}\mathrm{e}^{\mathrm{j}\Omega t}\}$. Then the current becomes

$$\hat{I} = \frac{\mathrm{j}\Omega C_0}{1 - C_0 \sum_i \frac{V_{\mathrm{R}i}^2}{k_{ii} - m_{ii}\Omega^2}} \hat{V}. \tag{21}$$

The infinite sum in the denominator is a series expansion of tan b (Ikeda 1996), thus the current is identical to

$$\hat{I} = \frac{\mathrm{j}\Omega C_0}{1 - k^2 \frac{\tan b}{b}} \hat{V} \tag{22}$$

with the parameters

$$k^2 = \frac{h^2}{\beta^{\mathrm{S}} c^{\mathrm{D}}} \quad \text{and} \quad b = \frac{\lambda l}{2}. \tag{23}$$

In literature the same result is obtained by direct solution of eq. 6 with an applied voltage. But the modal series expansion is much more flexible, as other loads and excitations may be considered as well. Furthermore this formulation will be the stepping stone for the modal reduction of systems with a finite number of degrees of freedom.
The electrical network, that is depicted in Figure 2(c) consists of one capacitive branch and parallel piezoelectric branches. Without damping and load it has the electrical input admittance

$$\frac{\hat{I}}{\hat{U}} = \mathrm{j}\Omega C_0 + \frac{1}{\frac{-1}{\mathrm{j}\Omega C_0} + \left(\sum_i \frac{1}{\mathrm{j}\Omega L_i + 1/(\mathrm{j}\Omega C_i)}\right)^{-1}}. \tag{24}$$

In order to uncover the relation to the modal series expansion eq. 21 is expanded and rearranged. Comparison of coefficients gives a constant inductivity

$$L_i = \frac{m_{ii}}{\alpha_i^2} \quad \text{and } C_i = \frac{\alpha_i^2}{k_{ii}} = \frac{1}{L\omega_i^2}, \tag{25}$$

where the factor $\alpha_i = C_0 V_{\mathrm{R}i}$ represents the coupling between the mechanical and electrical domain. The harmonic movement within a certain frequency range is dominated only by a few modes. Modes with a higher frequency than the excitation frequency behave like a capacitance. Their influence is concentrated into one residual capacitance ΔC. The summation of all capacities leads to the limit $\pi^2/8$ (Lenk et al. 2011). With p considered modes

Table 1: Modal parameters of the piezoelectric rod.

Open circuited modes	Short circuited modes
$m_{ii} = \frac{\rho A l a_i^2}{2}$	$m_{ii} = \frac{A\rho}{2}\left(l - \frac{\sin(\lambda_i l)}{\lambda_i}\right)$
$V_{\mathrm{R}i} = \begin{cases} -2ha_i, & \text{if } i \text{ odd} \\ +2ha_i, & \text{if } i \text{ even} \end{cases}$	$Q_{\mathrm{R}i} = \frac{2hA}{l\beta^{\mathrm{S}}} w(\frac{l}{2})$
$\alpha_i = C_0 V_{\mathrm{R}i}$	$\alpha_i = Q_{\mathrm{R}i}$
$\omega_i = \sqrt{c^{\mathrm{D}}/\rho}\lambda_i$	, $k_{ii} = m_{ii}\omega_i^2$, $C_0 = \frac{A}{l\beta^{\mathrm{S}}}$

the residual capacitance is

$$\Delta C = \left(\frac{\pi^2}{8} - \sum_{\mathrm{i}=1}^{\mathrm{p}} \frac{1}{(2i-1)^2}\right) C_1. \tag{26}$$

It is remarkable that the capacitance $C_0 + \Delta C$ of the EQC depends on the number of considered modes, in other words, the equivalent capacity is in general not equal to the static capacity.

Discretization with Short-Circuited Modeshapes

The short-circuited mode shapes do not contribute any voltage, but each mode shape causes a reaction charge Q_{R}. According to eq. 3 any applied voltage V results into an additional charge, therefore the total charge is

$$Q = \sum_{\mathrm{i}} Q_{\mathrm{R}i} q_i + C_0 V. \tag{27}$$

The voltage also performs a work W with the variation $\delta W = V\delta Q = w\delta\mathbf{q}^{\mathrm{T}}\mathbf{Q}_{\mathrm{R}} + C_0\delta V$. In this expression the variation of the voltage is not independent and depends on the variations of the charge or the displacement. The short-circuited modeshapes do not complete the half wavelength as the open circuited modeshapes do. Thus the discretized inner energy leads to the stiffness matrix

$$\mathbf{K}_{\mathrm{qq}} = Ac^{\mathrm{D}} \int_{-l/2}^{l/2} \mathbf{W}'\mathbf{W}'^{\mathrm{T}}\,\mathrm{d}z - \frac{\beta^{\mathrm{S}} l}{A} \mathbf{Q}_{\mathrm{R}}\mathbf{Q}_{\mathrm{R}}^{\mathrm{T}} = \mathbf{diag}(k_{ii}), \tag{28}$$

which is again orthogonal as shown in the appendix. The mass matrix is identical to the open circuited case and the piezoelectric coupling follows from the variation of work, where only the variations of the displacements are considered. The algebraic signs follow directly from the calculations. Together with eq. 27 a system of differential

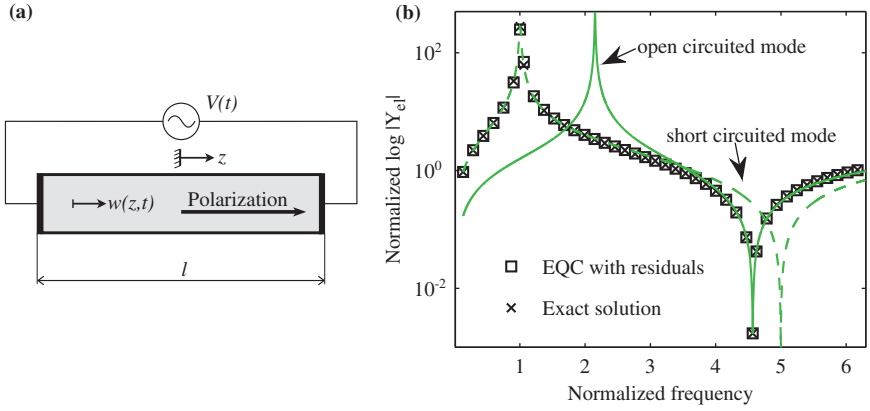

Figure 1: (a) Piezoelectric Rod, with the time t and position z dependent displacement $w(z, t)$ (b) Logarithmic electrical admittance for different series expansions.

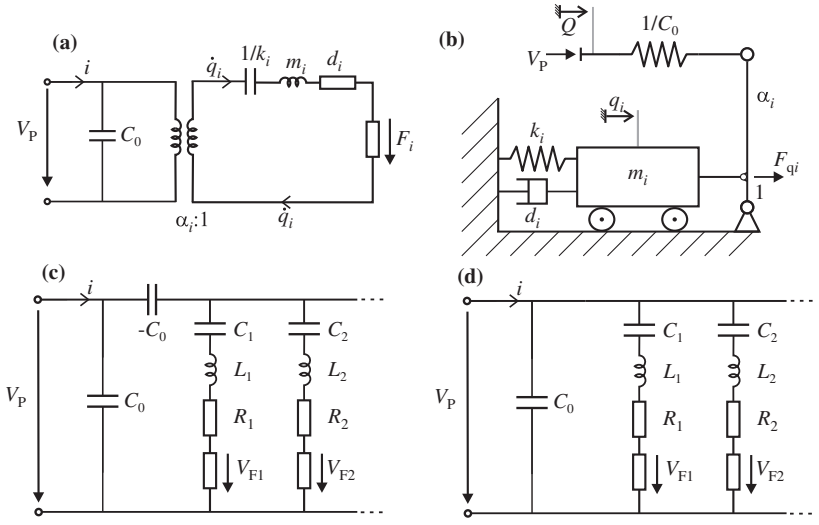

Figure 2: (a) Circuit with one short circuited mode and a transformer between mechanical and electrical domain (b) Mechanical representation of the circuit with one mode Kandare and Wallaschek (2002) (c) Circuit with many open circuited modes. The voltage $V_{F1} = \alpha_1 F_1$ represents the modal loading. The residual capacitance is included in the piezo capacitance. (d) Circuit with many short circuited modes. All four equivalent circuits utilize electrical and mechanical lumped parameters: capacity C_i, inductance L_i, resistance R_i, stiffness k_i, mass m_i, damper d_i and the electromechanical transfer factor α_i. Further, V_P represents the Voltage across the piezoelectric element, i and Q the corresponding current and charge, q_i is a mechanical modal displacement and F represent forces.

equations

$$\begin{bmatrix} \mathbf{M}_{qq} & \mathbf{0} \\ \mathbf{0} & 0 \end{bmatrix} \begin{pmatrix} \ddot{\mathbf{q}} \\ \ddot{V} \end{pmatrix} + \begin{bmatrix} \mathbf{K}_{qq} & -\mathbf{Q}_R \\ \mathbf{Q}_R^T & C_0 \end{bmatrix} \begin{pmatrix} \mathbf{q} \\ V \end{pmatrix} = \begin{pmatrix} \mathbf{F}_m \\ Q \end{pmatrix}, \quad (29)$$

is formed, where the voltage appears as an independent variable. The system is equivalent to the system in Figure 2(d), where no serial capacitance is needed within the piezoelectric branch compared to Figure 2(c). Obviously the two different classical equivalent networks with and without a serial capacitance are in accordance with a series expansion with the short-circuited and open-circuited modeshapes respectively. The input admittance for the short-circuited case is

$$\frac{\hat{I}}{\hat{U}} = \mathrm{j}\Omega C_0 + \mathrm{j}\Omega \sum_i \frac{Q_i^2}{k_{ii} - m_{ii}\Omega^2}. \quad (30)$$

Figure 1(b) shows the slightly damped electrical input admittance for the first longitudinal mode. The series expansion with the first open-circuited mode fits the reference solution in antiresonance exactly. The expansion with the first short-circuited mode described fits the resonance respectively. The residual capacitance strongly improves the quality of the short-circuited approximation. The damping in the plots is introduced by a complex youngs modulus.

Finite Element Model Order Reduction

Technical piezoelectric systems are more complex than the piezoelectric rod discussed in the section before. But the variational principle eq. 1 still holds and the system may be discretized with a commercial finite-element program. The resulting equations of motion

$$\begin{bmatrix} \mathbf{M} & \mathbf{0} \\ \mathbf{0} & \mathbf{0} \end{bmatrix} \begin{pmatrix} \ddot{\mathbf{x}} \\ \ddot{\mathbf{V}} \end{pmatrix} + \begin{bmatrix} \mathbf{D} & \mathbf{0} \\ \mathbf{0} & \mathbf{0} \end{bmatrix} \begin{pmatrix} \dot{\mathbf{x}} \\ \dot{\mathbf{V}} \end{pmatrix} \cdots + \cdots + \begin{bmatrix} \mathbf{K}_{\mathrm{xx}} & \mathbf{K}_{\mathrm{xe}} \\ \mathbf{K}_{\mathrm{xe}}^{\mathrm{T}} & -\mathbf{K}_{\mathrm{ee}} \end{bmatrix} \begin{pmatrix} \mathbf{x} \\ \mathbf{V} \end{pmatrix} = \begin{pmatrix} \mathbf{F}_{\mathrm{x}} \\ -\mathbf{Q} \end{pmatrix} \tag{31}$$

once again have a singular mass matrix. Note that in this representation multiple electrodes are included as well. In accordance with many FE-programs the direction of counting is chosen to be negative for the charge, in order to guarantee symmetric matrices. To avoid any confusion with the modal displacements, the vector of physical displacements here is named $\mathbf{x}$.

Discretization with Short-Circuited Modeshapes

The mechanical part of the short-circuited modeshapes is grouped into the modal matrix $\mathbf{\Phi}$. The mechanical modeshapes together with the electrical voltages form the transformation matrix

$$\begin{pmatrix} \mathbf{x} \\ \mathbf{V} \end{pmatrix} = \begin{bmatrix} \mathbf{\Phi} & \mathbf{0} \\ \mathbf{0} & \mathbf{1} \end{bmatrix} \begin{pmatrix} \mathbf{q} \\ \mathbf{V} \end{pmatrix}. \tag{32}$$

The internal electrical voltage may still be in $\mathbf{z}$ or the degrees of freedom are statically condensed employing the Guyan reduction before. However, in the modal representation the internal electrical field is described by the modal coordinates $\mathbf{q}$. After transformation and left multiplication of the transposed transformation matrix the reduced problem becomes

$$\begin{bmatrix} \mathbf{M}_{\mathrm{qq}} & \mathbf{0} \\ \mathbf{0} & \mathbf{0} \end{bmatrix} \begin{pmatrix} \ddot{\mathbf{q}} \\ \ddot{\mathbf{V}} \end{pmatrix} + \begin{bmatrix} \mathbf{D}_{\mathrm{qq}} & \mathbf{0} \\ \mathbf{0} & \mathbf{0} \end{bmatrix} \begin{pmatrix} \dot{\mathbf{q}} \\ \dot{\mathbf{V}} \end{pmatrix} \cdots + \cdots + \begin{bmatrix} \mathbf{K}_{\mathrm{qq}} & -\mathbf{Q}_{\mathrm{R}} \\ \mathbf{Q}_{\mathrm{R}}^{\mathrm{T}} & \mathbf{K}_{\mathrm{ee}} \end{bmatrix} \begin{pmatrix} \mathbf{q} \\ \mathbf{V} \end{pmatrix} = \begin{pmatrix} \mathbf{F}_{\mathrm{q}} \\ \mathbf{Q} \end{pmatrix}, \tag{33}$$

with the abbreviations

$$\begin{aligned} \mathbf{M}_{\mathrm{qq}} &= \mathbf{\Phi}^{\mathrm{T}}\mathbf{M}\mathbf{\Phi} = \mathbf{diag}(m_{\mathrm{ii}}) \\ \mathbf{D}_{\mathrm{qq}} &= \mathbf{\Phi}^{\mathrm{T}}\mathbf{D}\mathbf{\Phi} = \mathbf{diag}(d_{\mathrm{ii}}) \\ \mathbf{K}_{\mathrm{qq}} &= \mathbf{\Phi}^{\mathrm{T}}\mathbf{K}_{\mathrm{xx}}\mathbf{\Phi} = \mathbf{diag}(k_{\mathrm{ii}}) \\ \mathbf{Q}_{\mathrm{R}} &= -\mathbf{\Phi}^{\mathrm{T}}\mathbf{K}_{\mathrm{xe}} \\ \mathbf{K}_{\mathrm{ee}} &= \mathbf{diag}(C_{0i}) \\ \mathbf{F}_{\mathrm{q}} &= \mathbf{\Phi}^{\mathrm{T}}\mathbf{F}_{\mathrm{x}} \\ \mathbf{Q} &= [Q_1 \ldots Q_m]^{\mathrm{T}}. \end{aligned} \tag{34}$$

A similar result with a slightly different derivation is obtained by (Hohl et al. 2009). Król (2011) also applies a modal transformation to the discrete FE-model that shows the connection to some EQCs as well. The scaling of the eigenvectors is arbitrary, but from a computational point of view a mass normalization is convenient. Thus the modal mass matrix $\mathbf{M}_{\mathrm{qq}}$ becomes the unity matrix ($m_{ii} = 1$) and the modal stiffness matrix $\mathbf{K}_{\mathrm{qq}}$ is filled with the eigenfrequencies ($k_{ii} = \omega_i^2$). The modal damping matrix $\mathbf{D}_{\mathrm{qq}}$ contains the modal damping ratios $d_{ii} = 2D_i\omega_i$, which theoretically follow from a damped modal analysis. But as model-based damping values are often quite inaccurate, it is often more useful to define the modal damping ratios directly. Also the modal reaction charge $\mathbf{Q}_{\mathrm{R}}$ is a direct result of the FE-analysis. Very often the displacement of a certain working point is of special interest. If the modes are normalized with respect to this point, the modal amplitudes will be identical to the physical displacement at this point. Thus any loading at a given working point will be considered with its physical values. This normalization is also assumed implicitly when the model is identified experimentally. In general the modal forces $\mathbf{F}_{\mathrm{q}}$ and the piezo capacitances C_{0i} of each electrode require separate calculations. While the calculation of the modal forces is straightforward, the piezo capacitances may be directly read from the system matrices. If this is not possible within the FE-program, a separate static analysis would be necessary. But it will be shown in further discussion, that the piezo capacitance is best determined together with the residual capacitance.

Discretization with Open-Circuited Modeshapes

The open-circuited modeshapes are obtained by a modal analysis of the undamped system without any electrical boundary conditions. The mass matrix is singular and the electrical degrees of freedom are statically condensed with the Guyan reduction. These modeshapes are used within the modal transformation $\mathbf{x} = \mathbf{\Phi q}$. The resulting

uncoupled set of modal equations do not contribute any charge. The physical deformation **x** is solely described by the modal coordinates, therefore any charge leads to an additional voltage. According to the second row of eq. 31 the total voltage is

$$\mathbf{V} = \mathbf{K}_{ee}^{-1}\mathbf{K}_{xe}^{T}\mathbf{\Phi}\boldsymbol{q} + \mathbf{K}_{ee}^{-1}\mathbf{Q} = \mathbf{V}_{R}^{T}\mathbf{q} - \mathbf{K}_{ee}^{-1}\mathbf{Q}, \tag{35}$$

with the transposed modal reaction voltages

$$\mathbf{V}_{R}^{T} = \mathbf{K}_{ee}^{-1}\mathbf{K}_{xe}^{T}\mathbf{\Phi}\boldsymbol{q}. \tag{36}$$

The additional voltage also causes additional modal forces

$$\mathbf{F}_{qe} = \mathbf{\Phi}^{T}\mathbf{K}_{xe}\mathbf{K}_{ee}^{-1}\mathbf{Q} = -\mathbf{V}_{R}\mathbf{Q}. \tag{37}$$

The additional modal forces are included in the modal stiffness matrix. With eq. 35 and the abbreviations of eq. 34 the reduced system results as

$$\begin{bmatrix} \mathbf{M}_{qq} & \mathbf{0} \\ \mathbf{0} & \mathbf{0} \end{bmatrix}\begin{pmatrix} \ddot{\mathbf{q}} \\ \ddot{\mathbf{Q}} \end{pmatrix} + \begin{bmatrix} \mathbf{D}_{qq} & \mathbf{0} \\ \mathbf{0} & \mathbf{0} \end{bmatrix}\begin{pmatrix} \dot{\mathbf{q}} \\ \dot{\mathbf{Q}} \end{pmatrix} \ldots + \ldots + \begin{bmatrix} \mathbf{K}_{qq} & \mathbf{V}_{R} \\ \mathbf{V}_{R}^{T} & \mathbf{K}_{ee}^{-1} \end{bmatrix}\begin{pmatrix} \mathbf{q} \\ \mathbf{Q} \end{pmatrix} = \begin{pmatrix} \mathbf{F}_{q} \\ \mathbf{V} \end{pmatrix}. \tag{38}$$

The expansions with respect to the short- and to the open-circuited modes again lead to equations that describe the Butterworth Van Dyke EQCs. With the application to FE-models the procedure also gains its value for complex technical problems.

Residual Terms

The frequency response of a technical system is evaluated within a certain frequency range only. The eigenmodes out of this range only contribute little to the response and therefore are often truncated. For discrete models the influence of higher modes can be approximated by residual terms, as shown already for the piezoelectric rod. Porfiri et al. (2007) also found, that the piezo capacitance depends on the number of considered modes. From the matrix representation eq. 33 the electrical input admittance is expanded with the first m eigenmodes

$$\begin{aligned} \frac{\hat{I}}{\hat{V}} &= \mathrm{j}\Omega\left(C_0 + \sum_{i=1}^{m}\sum_{i=m+1}^{n}\frac{Q_{Ri}^2}{k_{ii} + \mathrm{j}\Omega d_{ii} - m_{ii}\Omega^2}\right) \\ &\approx \mathrm{j}\Omega\left(C_0 + \sum_{i=1}^{m}\frac{Q_{Ri}^2}{k_{ii} + \mathrm{j}\Omega d_{ii} - m_{ii}\Omega^2} + \sum_{i=m+1}^{n}\frac{Q_{Ri}^2}{k_{ii}}\right) \\ &\approx \mathrm{j}\Omega\left(C_0 + \Delta C + \sum_{i=1}^{m}\frac{Q_{Ri}^2}{k_{ii} + \mathrm{j}\Omega d_{ii} - m_{ii}\Omega^2}\right). \end{aligned} \tag{39}$$

The truncated modes are subcritical and behave like a spring or capacitance, assuming they are weakly damped. Therefore all truncated modes are approximated by one residual capacitance ΔC, which is best identified with a static or harmonic solution of the complete model. The residual capacitance follows simply from the difference of the complete and reduced solution. From a practical viewpoint the residual capacitance is best identified together with the capacitance C_0. With the harmonic reaction load $Q_{R,1V}$ at 1 V voltage the total capacitance follows as

$$C_0 + \Delta C = Q_{R,1V} - \sum_{i=1}^{m}\frac{Q_{Ri}^2}{k_{ii} + \mathrm{j}\Omega d_{ii} - m_{ii}\Omega^2}, \tag{40}$$

which can directly be used within the EQC. The total capacitance can be calculated with a static analysis as well. In addition to the approximation of higher modes, modes below the evaluated frequencies also contribute to the admittance. Theoretically the same summation as above is possible for the lower modes and a definition for a residual inductance mass is respectively possible. Mostly only a few lower modes are truncated and their effect is not very strong. Therefore these residual inductances are not introduced here.

Summarizing the preceeding explanations, the typical model order reduction of piezoelectric systems with a finite number of degrees of freedom can be stated as follows:

1. A modal analysis with mass normalized eigenvectors gives the eigenfrequencies $\omega_i^2] = k_{ii}/m_{ii}]$. In the case of short-circuited electrodes the piezoelectric coupling is defined by the modal reaction charges Q_{Ri} and in the open-circuited case by the reaction voltages V_{Ri}. All mechanical entries of the mass matrix are $m_{ii} = 1$ and the damping matrix is best defined manually. The modal forces follow from the physical forces according to $\mathbf{F}_q = \mathbf{\Phi}^T\mathbf{F}_x$. Hence the eigenvectors have to be evaluated at the points of force application only.
2. The total capacitance results from a static analysis with 1 V voltage as

$$C_0 + \Delta C = Q_{R,1V} - \sum_{i=1}^{m}\frac{Q_{Ri}^2}{\omega_i^2}. \tag{41}$$

In the case of a reduction with open-circuited modes, a further static analysis step without piezoelectric coupling is required, in order to isolate the value of C_0.

Experimental Identification

The preceding modal parameter extraction is based on a model of the piezoelectric device. A direct identification of a physical systems needs a different approach, as most often only the frequency response data are available. Based on a harmonic voltage excitation, the current and velocity amplitudes are measured and the admittances are used for the extraction of the EQC parameters. The identification procedure is well described in literature for one isolated mode, but to the knowledge of the authors no reports of an identification procedure for many modes exists. First the case of one mode is discussed separately and then the procedure is generalized for many modes.

Identification with One Mode

The parameter identification in the vicinity of one isolated mode is reported by different authors. The following identification procedure is based on (Richter et al. 2009). The procedure can be interpreted as a circle fit of the complex admittance locus. The circle offset on the imaginary axis of the electrical admittance is directly related to the piezo capacitance and the proportion of the radius of the electrical and mechanical admittance defines the electromechanical coupling.

- For weakly damped systems the inductance and the capacitance compensate each other and only the resistor R_1 is effective. The real part of the admittance is the inverse of the resistor: $R_1 = 1/\mathrm{Re}\{Y(\omega_{S_1})\}$.
- The quality factor Q_{m_1} is measured with the frequencies at -3 dB ω_a and ω_b around the serial resonance ω_{S1} and is related to the inductance L_1 with:

$$Q_{m_1} = \frac{\omega_{S_1}}{\omega_b - \omega_a} \tag{42}$$

$$L_1 = Q_{m_1} \frac{R_1}{\omega_{S_1}}. \tag{43}$$

- The capacitance is determined by the resonance frequency

$$C_1 = \frac{1}{L_1 \omega_{S_1}}. \tag{44}$$

- The distance between serial and parallel resonances delivers the piezo capacitance of the model

$$\frac{C_1}{C_0} = (\frac{f_{P_1}}{f_{S_1}})^2 - 1. \tag{45}$$

- The factor α_1, representing the coupling between the mechanical and electrical domains, is the ratio of the mechanical velocity and the input current in resonance

$$\alpha_1 = \frac{\hat{v}}{\hat{I}}. \tag{46}$$

Identification with Two Modes

If a second mode exists relatively close to the first mode, the frequencies of anti resonance (or parallel resonance) will be perturbed, while the serial resonance frequencies remain unperturbed. This becomes clear with eq. 39, because the pole of the admittance, and hence the serial resonance, is not affected by C_0, while the roots and hence the parallel resonances are strongly influenced by the piezo capacitance. With the same argumentation, the values of R_i L_i and C_i can be identified separately for each serial resonance. For each mode also a piezo capacitance

$$C_{0i}^* = \frac{C_i}{\left(\frac{f_{Pi}}{f_{Si}}\right)^2 - 1}, \tag{47}$$

is identified, but the complete model consists only of one capacitance C_0. In order to clarify the influence of the piezo capacitance a typical admittance curve with two modes between 20 and 21 kHz is depicted in Figure 3(a). The true admittance curve of the system with $C = C_0$ is plotted together with two identified admittance curves, respectively identified with the piezo capacitances of both modes $C = C_{01}^*$ and $C = C_{02}^*$, where the star denotes an approximated value. It can be noticed that with $C = C_{01}^*$ the parallel resonance frequencies are underestimated, while with $C = C_{02}^*$ the parallel resonance frequencies are overestimated. Below its resonance frequency, the second mode behaves like a capacitance and hence the identified piezo capacitance at the first mode C_{01}^* appears to be higher than the true piezo capacitance C_0. On the other hand the first mode behaves like an inductance for frequencies higher than the first resonance and the identified piezo capacitance of the second C_{02}^* mode is lower than C_0. These relations are absolutely analogue to the concept of residual terms discussed before and can be summarized in the inequality

$$C_{02}^* < C_0 < C_{01}^*. \tag{48}$$

The identified frequencies of the parallel resonances obey accordingly

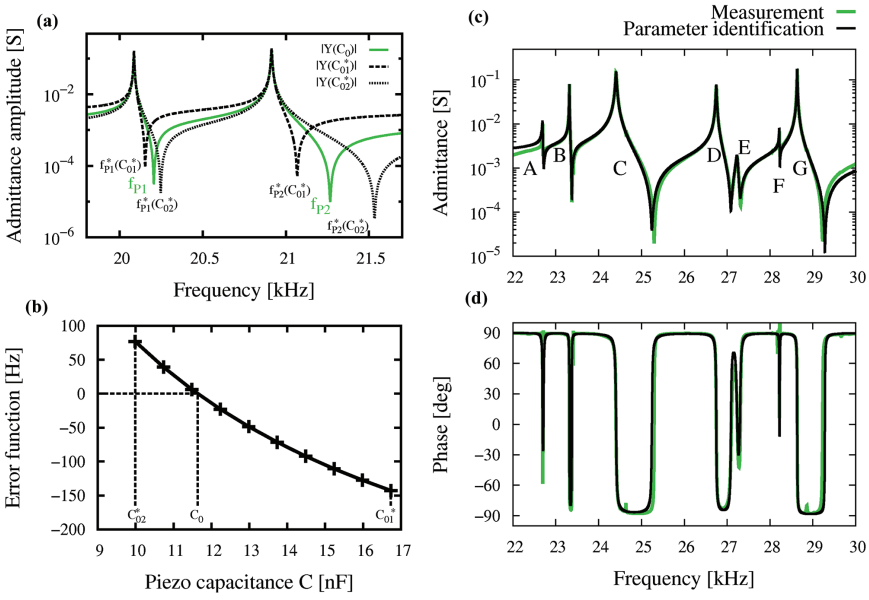

Figure 3: (a) Typical electrical admittance (green) and identified admittances. With $C = C_{01}^*$ the parallel resonances are underestimated, with $C = C_{02}^*$ the parallel resonance frequencies are overestimated. (b) The difference of measured and model based parallel resonance frequency is minimized. (c) Measured and identified amplitude of the admittance (d) Measured and identified phase of the admittance.

$$f_{Pi}^*(C_{01}^*) < f_{Pi} < f_{Pi}^*(C_{02}^*). \tag{49}$$

The error function

$$error(C) = (f_{P1}^*(C) - f_{P1}) + (f_{P2}^*(C) - f_{P2}^*) \tag{50}$$

is used to find the optimal piezo capacitance $C = C_0$. From a principle viewpoint the error only needs to be evaluated for one mode, but in order to consider the influence of close modes, that have not been identified, the error is considered for all modes. As depicted in Figure 3(b) the error function needs only to be evaluated between C_{01}^* and C_{02}^*. Because of the smooth function an interpolation minimizes the numerical effort.

Identification with More than Two Modes

The identification of a system with many modes follows the same patterns as the identification of a system with two modes.

The constants L_i, C_i and R_i are again identified separately for each resonance and the piezo capacitance results from the minimization of the error function. Modes stuck between neighbour modes are perturbed and their parallel frequency is shifted either to a lower or a higher frequency. It is again sufficient to consider the difference of measured and approximated resonance frequency for one mode only. But due to the influence of neighbor modes the results will be improved, if the error is considered for all modes. The tuning range of C is determined by the extremal values of the identified capacitances.

Figure 3(c) and (d) depict the measured and identified admittances of an ultrasonic welding system with seven modes in the frequency range from 22 to 30 kHz. A good correlation can be noticed between measured and identified admittances. Even the small mode E, that perturbs the mode D, is identified properly and the assumption of independent modal parameters holds. The only remarkable difference between measured and identified signal occurs at the frequency limits. Therefore modes in the vicinity of the interesting frequency range should be identified as well.

Examples

The introduced methods are demonstrated with some examples that also contain additional aspects. In the first two examples general aspects such as loading and the quality of the modal basis are discussed. The third and the fourth example present concrete technical applications of the proposed methods.

Loaded Piezoelectric Rod

Every piezoelectric actuator drives some process that should be considered within the model. The integration

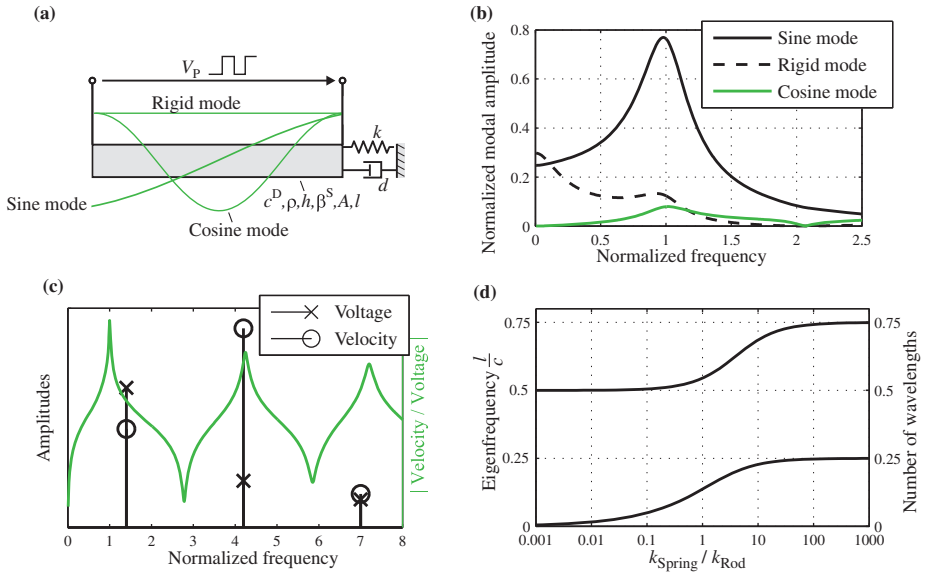

Figure 4: (a) Piezoelectric rod with a damper representing the process and the first short-circuited modeshapes. (b) First modal amplitudes with the parameters $c^D = 1.6\ 10^{11}\ \frac{N}{m^2}$, $\rho = 8850\ \frac{kg}{m^3}$, $\beta^S = 1.6\ 10^8\ \frac{Vm}{As}$, $h = 4\ 10^9\ \frac{V}{m}$, $V_P = 1$ V, $A = 3.1\ 10^{-4}$ m^2, $l = 0.005$ m, $k = 0$ and d equal to the half wave impedance. (c) Multi harmonic response characteristic. (d) Influence of a spring on the open-circuited modeshape and eigenfrequency.

of the process model is exemplified for a piezoelectric rod, but an analogue procedure can be applied to any FE-model. If the loading acts at one position only, the modeshapes can be normalized with respect to this point and the model of the physical process can directly be included into the reduced model.

The piezoelectric rod with load is depicted in In Figure 4(a). In contrast to the previous calculations here not only the sine, but also the cosine and rigid body modeshapes are used in the modal expansion. The eigenfrequency of the rigid body mode is zero and the modal mass is identical to the physical mass with the proposed scaling. The wavenumbers of the short circuited sine modeshapes follow from the transcendental eq. 10 and after some calculations the wavenumbers of the cosine modes simply write as $\lambda_{ci} = i\pi$. The damper performs the virtual work

$$\begin{aligned} \delta W &= F\delta w \\ &= (-d\ \dot{\mathbf{q}}^T\ \mathbf{W}_L)\,(\mathbf{W}_L^T\ \delta\mathbf{q}) \\ &= -\mathbf{D}\ \dot{\mathbf{q}}\ \delta\mathbf{q}, \end{aligned} \tag{51}$$

with the modal displacements at the position of load $\mathbf{W}_L$. The damping matrix $\mathbf{D}$ is fully populated with d in every entry. It is clear that the local damper couples each mode with every other mode. A representation of this coupling within a simple EQC will only be possible, if all α_i are identical. Although this holds in this example, in general this is not true. The coupling of the modes is also illustrated in Figure 4(b). Only the sine mode is electrically excited, but due to the damper also the rigid body mode and the cosine mode also contribute to the resulting movement. The importance of the multi modal modeling becomes especially clear in the case of non sinusoidal excitations. Figure 4(c) shows the first harmonic contributions of a rectangular voltage signal. Depending on the piezoelectric structure the second harmonic meets a resonance and is strongly gained compared to the base amplitude.

If the influence of the load is strong, it can change the vibrations of the rod. The open-circuited eigenfrequencies of a loaded piezoelectric rod are the zeros of

$$b \tan b = \frac{k_L}{k_{Rod}} \tag{52}$$

with the total stiffness of the rod $k_{Rod} = c^D A/l$ and the abbreviation $b = \omega l/c$. A local damper has only a minor effect on the eigenfrequency, but a local stiffness or mass changes the eigenfrequency significantly. In Figure 4(d) the change of the open-circuited eigenfrequency for variation of the spring is illustrated. The limiting case of a very high stiffness is equivalent to a clamped boundary condition. The change of the resulting modeshapes gives raise to the question of the quality of the modal basis, that is discussed in the next example.

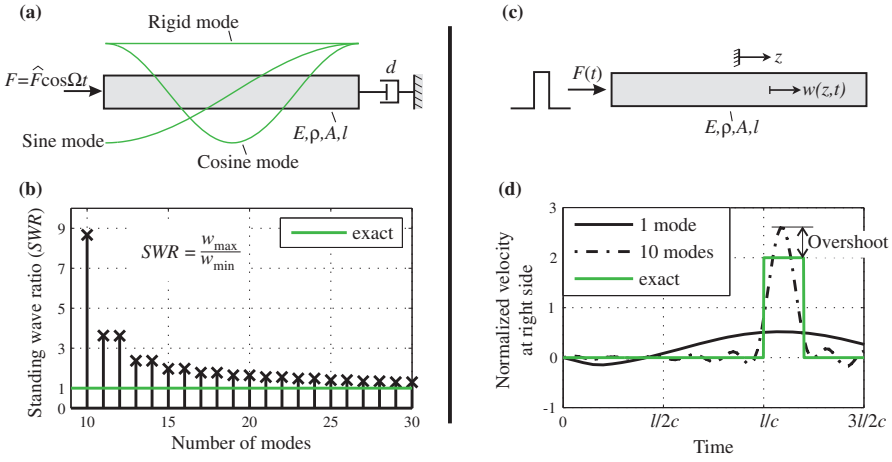

Figure 5: (a) Force excited passive rod with local damper (b) Standing wave ratio for different number of considered modes and $\Omega = f_{10}$ (c) Passive rod with a force pulse (d) Velocity at the right side. The velocity is normalized to the exact result inside the rod.

Quality of Modal Basis

Although a local damper has only a minor influence on the eigenfrequency, it nevertheless changes the vibration shape. By increasing the damping, the ratio of reflected and absorbed waves at the damped border decreases and hence the standing wave ratio also decreases. If the damping value equals the wave impedance $d = Z_W = A\sqrt{E\rho}$ the damper will absorb all waves and the standing wave ratio becomes one. This vibration shape cannot be mapped with only one mode and therefore several modes are necessary. Figure 5(b) shows the resulting standing wave ratio for a different number of considered modes. The rod is excited with the 10^{th} resonance frequency and therefore the resulting wavelength equals the wavelength of the 10^{th} mode as well. With only ten modes the approximation is inaccurate, but when an increasing number of modes is considered it improves and converges to the exact solution.

Due to the modal expansion an excitation at one certain position causes an effect on the complete system instantaneously. In Figure 5(d) the velocity at the right end of a bar is plotted for a force pulse at the left side. In reality the pulse travels with sonic velocity $c = \sqrt{E/\rho}$, but in the reduced model a deflection occurs instantaneously. The quality of approximation improves with the number of modes as well, but in contrast to the prior example the approximation does not converge to the exact solution. This is related to Gibb's phenomenon that applies to nonsmooth functions. The optimal approximation of a given rectangular deflection with the eigenfunctions shall be investigated. The eigenfunctions of the free rod form a system of orthogonal functions $1, \sin(\frac{\pi}{l}z), \cos(\frac{2\pi}{l}z), \sin(\frac{3\pi}{l}z)$.... This series is similar to a Fourier series, but for one wavenumber respectively frequency here only one harmonic function exists. The amplitude of each function is the scalar product of the deflection $p(z)$ and the eigenfunction $e_i(z)$

$$q_i = \frac{1}{2l}\int_{-l/2}^{l/2} p(z)e_i(z)\,\mathrm{d}z. \tag{53}$$

The approximated deflection $w(z) \approx \sum_i q_i e_i(z)$ converges to an overshoot of 9%, which is also obtained by a Fourier series of a rectangular pulse. Accordingly, the amplitudes of the missing functions become zero in the Fourier expansion as well.

Ultrasonic Grubber

In agricultural tillage the friction between the grubbers tine and the soil is a limiting factor. To overcome this problem longitudinal ultrasonic vibrations are induced into the tine in order to reduce the resulting friction forces. In this contribution only the effect of the frictional contact on the structural vibrations and hence on the electrical input admittance is discussed. The principles of friction reduction are, for example, explained by (Littmann et al. 2001) and further data on the performance of the ultrasonic grubber is published by (Kattenstroth et al. 2011). The design of the grubber is depicted in Figure 6(a). The length of the friction contact depends on the depth of the grubber. The effect of the physical friction force on the modal vibration is position dependent. In general the modal force is the scalar product of the physical force and the vibration shape. With only one mode and zero driving velocity the modal friction force becomes

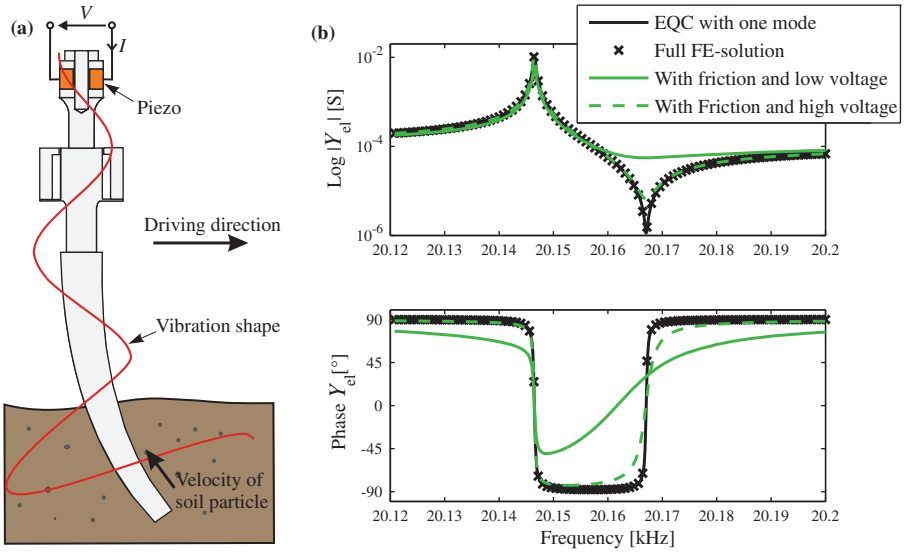

Figure 6: (a) Sketch of the ultrasonic grubber (b) Frequency response with and without friction between tine and soil.

$$\begin{aligned} F_q &= -\int_A \mathbf{\Phi} \cdot \frac{\mathbf{\Phi}}{|\mathbf{\Phi}|}\, \mu p_N\, \mathrm{sgn}(\dot{q})\, \mathrm{d}A \\ &= -\int_A |\mathbf{\Phi}|\, \mathrm{d}A\, \mu p_N\, \mathrm{sgn}(\dot{q}) \\ &= -r\, \mathrm{sgn}(\dot{q}), \end{aligned} \tag{54}$$

where p_N is the constant normal pressure and μ the constant friction coefficient. The integral of the friction area has to be approximated by the FE-program. The values of the integral for the working mode and the friction pressure are combined into the resulting constant modal friction force r, which is always in the opposite direction of the velocity. In the general case with more modes or a non zero driving velocity a numerical solution is necessary. But these strong assumptions allow an analytical solution employing the harmonic balance method (Popov and Paltov 1960). Within the harmonic balance approach the non-smooth friction force is assumed to be harmonic. With the ansatz $q(t) = \hat{q}\cos(\Omega t - \Psi)$ the exact friction force is calculated and developed into a Fourier series. From the first harmonic contribution of the non-smooth friction force an equivalent amplitude depending damping is defined as

$$d^* = \frac{4r}{\pi\Omega\hat{q}}. \tag{55}$$

With the common variable name $Q_R = \alpha$, the governing equations of the EQC are

$$\begin{aligned} m\ddot{q} + \left[d + d^*(q)\right]\dot{q} + kq &= \alpha V \\ C_0 V + \alpha q &= Q. \end{aligned} \tag{56}$$

This is a common representation of the EQC, but it should be noted that due to the scaling of the eigenvectors the amplitude $\hat{q}$ is not identical to the physical movement at a certain position in general. In a classical identification of an EQC $\hat{q}$ would be scaled to meet the physical amplitude at a certain position. Though from a computational point of view a mass scaling with $m = 1$ is more convenient. The second order differential equation is solved analytically and the resulting charge and current are reconstructed afterwards. Figure 6(b) shows the resulting electrical admittance for different friction forces. The reduced solution without contact fits the harmonic FE-solution exactly. The equivalent damping coefficient decreases with increasing amplitude. Therefore the resonance is only slightly damped, while the antiresonance is much more affected by the friction damping. The non-symmetric electrical phase curve is characteristical for friction damped systems and is observed in experiments as well.

Base Excited Energy Harvester

During the last years energy harvesting applications attract increasing attention. Especially the base excited piezoelectric beam is a well discussed example in literature. Sodano et al. (2004) use the assumed modes method for the investigation of this example. Roundy and Wright (2004) and Twiefel et al. (2008) derive an EQC considering one mode. Analytical expressions of the EQC for a piezoeelctric beam are also found by (Al-Ashtari et al. 2012).

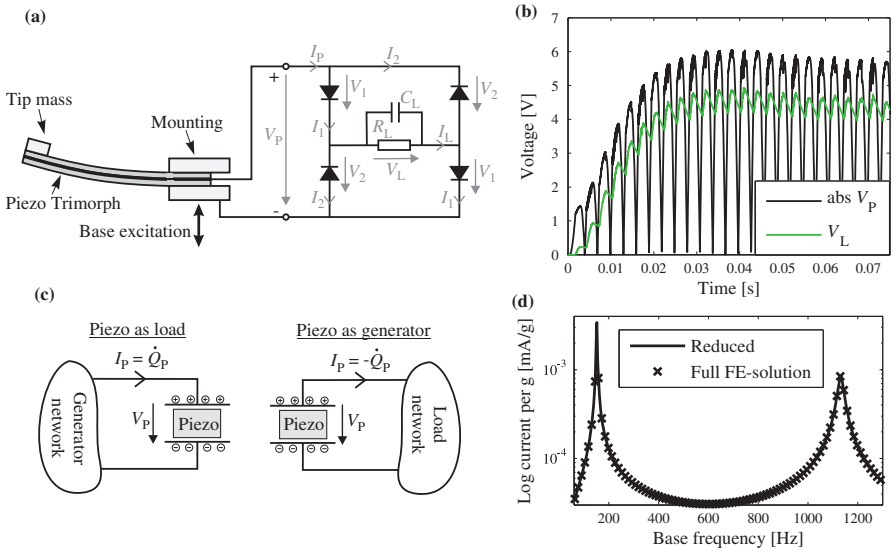

Figure 7: (a) Base excited piezoelectric energy harvester with full bridge rectifier network. (b) Resulting voltage at the piezo and the load. (c) Sign convention for electrical networks with a piezo as consumer or as generator. (d) Full finite element and reduced frequency response of the beam harvester with short circuited electrodes.

Elvin and Elvin (2009) first use non-orthogonal ansatz-functions and derive decoupled equations in a second step. An overview of some modelling approaches is given by (Erturk and Inman 2008). In contrast to the aforementioned work the derivation of an EQC in this paper starts with a finite element model. Thus the application of this model for arbitrary base excited structures is similar.

Instead of simulating the movement of the base directly, calculations are performed in the moving base reference frame. In this frame any acceleration $\mathbf{a}$ of the base is equivalent to the ith modal apparent force

$$F_{qi} = -\int_B \mathbf{\Phi}_i \cdot \mathbf{a}\, dm\,. \tag{57}$$

The modal analysis can be performed in the fixed reference frame. Here, the base excitation only appears as an external force. The electrical output of the piezo only depends on the strain inside the material and thus the superimposed movement of the reference frame is not important for the electrical output. Some authors use other modeling approaches for the base excitation, cf. (Erturk and Inman 2008) for a discussion on different approaches. The FE approximation of eq. 57 is often called the ith modal participation factor. Though in literature this term is also used more general as a modal force for an arbitrary loading. For example in the FE-program Ansys this closer defined participation factor is a standard output of a modal analysis and easily accessible. All other parameters of the EQC model are derived as described in the section before. To evaluate the quality of the model order reduction a full harmonic FE-analysis with base excitation is performed as a reference. The harmonic analysis is performed with a constant damping ratio $\zeta = 0.01$. Note that the stiffness proportional damping factor β is related to the modal damping ratio by $2\zeta_i = \beta\omega_i$. In order to achieve a constant damping ratio Ansys sets $\beta = 2\zeta/\Omega$ in a full harmonic analysis and hence updates the damping matrix every frequency step. In the reduced model the constant damping ratio is directly included as constant modal damping. Figure 7(d) shows the generated current per base acceleration with open electrodes. Two modes are considered within the reduction.

The piezoelectric trimorph, as depicted in Figure 7(a), is equipped with a tip mass and connected to a full bridge rectifier network. The resistive load has a parallel capacitance to achieve a smooth voltage. The same network is also discussed by (Roundy and Wright 2004) as well as (Elvin and Elvin 2009). The latter authors use the network simulation software SPICE for the analysis. This indicates a general procedure for attached electrical networks: the piezoelectric structure is modelled according to Figure 2 and the network is just attached. The full bridge rectifier is fundamental as well as still manageable, therefore the describing equations are derived in the following. Due to the symmetric structure of the network the voltages are pairwise identical. With the piezo voltage V_P and the voltage at the load V_L as independent state variables, the voltage at the nonlinear diodes follows from Kirchhoffs voltage law as

$$V_1 = \frac{1}{2}(V_P - V_L) \quad \text{and} \quad V_2 = \frac{1}{2}(V_P + V_L)\,. \tag{58}$$

Table 2: Equivalent parameters of the investigated harvester.

f_{eig}	Q_{R}	F_{q}	C_{P}	C_{L}	R_{L}
151 Hz	0.038 $\frac{\text{As}}{\text{m}}$	-0.0173 N	2.6 pF	13 pF	1 MΩ
1132 Hz	-0.1355 $\frac{\text{As}}{\text{m}}$	-0.0087 N			

The current in the diode is calculated with a piecewise linear model. Below the forward voltage $V_{\text{F}} = 0.6$ V the current is assumed as zero and for higher voltages the diode behaves like a resistor with $R = 10\ \Omega$. The currents I_{P} and I_{L} follow directly from the currents in the diodes. With this information the time derivatives of the state variables are

$$\begin{aligned} \dot{V}_{\text{P}} &= -\frac{I_{\text{P}}}{C_{\text{P}}} - \frac{1}{C_0}\mathbf{Q}_{\text{R}}^{\text{T}}\dot{\mathbf{q}} \\ \dot{V}_{\text{L}} &= \frac{I_{\text{L}}}{C_{\text{L}}} - \frac{V_{\text{L}}}{R_{\text{L}}C_{\text{L}}}. \end{aligned} \tag{59}$$

The algebraic sign of the current I_{P} in the former equation is non intuitive and is discussed following the patterns of (Tiersten 1969). In Figure 7(d) a positive voltage at the piezo-generator is sketched. The positive voltage is essentially connected with a positive charge on the upper electrode. Inside the dielectric piezo material the charge is not free and thus a growth of positive charge at the upper electrode leads to a current from the network to the piezo. Therefore positive current I_{P} is related to a decrease of the piezo charge and the relation $I_{\text{P}} = -\dot{Q}_{\text{P}}$ holds. If the piezo is driven as an actuator the sign convention between voltage and current normally is changed and the current is the positive derivative of the charge.

The voltages at the load and the piezo, together with the reduced piezoelectric model (Equation 33) are formed into a first order state space model, that can be straightforwardly numerically integrated. Figure 7(b) shows the transient response of the system at a fixed frequency of $1,1 f_1$ and a base acceleration amplitude of $a = 1\,\text{g}$. The capacitance is loaded when the piezo voltage exceeds the voltage at the capacitance plus the forward voltage. If the diodes are not conductive, the capacitance will be discharged by the resistance.

Conclusion

An extended model order reduction technique is applied to a continuous piezoelectric rod as well as to finite element models. The variational formulation of the piezoelectric rod is discretized using a Ritz-ansatz with the eigenfunctions. In order to simplify the expressions the electric displacement is used as the independent variable instead of the electric field. The discrete finite element model is transformed with linear matrix algebra. For both, the continuous and the discrete system, the voltage remains independent, in the case of short-circuited modes. In contrast, an expansion with the open-circuited modes leads to an independent charge. In the reduced systems the modal mechanical and the physical electrical degrees of freedom are always coupled with the modal electrical reactions. The influence of truncated higher modes is approximated by residual terms. With this approach arbitrary linear piezoelectric systems and loads are precisely and effectively simulated. Moreover the reduction method leads to the classical Butterworth Van Dyke equivalent circuits. For the piezoelectric rod it is shown, that even the parameters are identical. Therefore the widely used and trusted equivalent circuit approach is shown to be identical to the proposed model order reduction. This gives a better understanding of the equivalent circuit and also allows precise statements of how to consider any given load.

Appendix

Consider two eigensolutions of the eigenvalue problem eq. 8 with homogeneous boundary conditions

$$\begin{aligned} w_a'' + \lambda_a^2 w_a &= 0 \\ w_b'' + \lambda_b^2 w_b &= 0. \end{aligned} \tag{60}$$

After multiplying the first equation with w_b'', the second with w_a'', building the difference and integration of the resulting expression one obtains

$$0 = \int_0^l \lambda_a^2 w_a w_b'' - \lambda_b^2 w_a'' w_b \mathrm{d}z \tag{61}$$

$$= \left[\lambda_a^2 w_a w_b' - \lambda_b^2 w_a' w_b\right]_0^l + (\lambda_b^2 - \lambda_a^2)\int_0^l w_a' w_b'\ \mathrm{d}z. \tag{62}$$

With zero displacement or zero dielectric displacement boundary conditions the first difference expression is zero and hence also the integral vanishes for different eigenvalues. For zero voltage and at least one free boundary condition (Equation 7) the relation becomes

$$0 = (\lambda_b^2 - \lambda_a^2)\left[\int_0^l w_a' w_b' \mathrm{d}z - \frac{\beta^{\text{S}} l}{c^{\text{D}}} D_a D_b\right], \tag{63}$$

where D_a and D_b are the reaction dielectric displacements. Thus for zero voltage and force free boundary conditions the expression in the squared brackets vanishes for different eigenvalues.

The former equations define the stiffness-orthogonality for the piezoelectric rod. The mass orthogonality follows after multiplication of eq. 60 with w_a respectively w_b and an analog calculation for all considered boundary conditions as

$$0 = \int_0^l w_a w_b \, \mathrm{d}z \text{ for } a \neq b. \tag{64}$$

References

Al-Ashtari, W., M. Hunstig, T. Hemsel, and W. Sextro. 2012. "Analytical Determination of Characteristic Frequencies and Equivalent Circuit Parameters of a Piezoelectric Bimorph." *Journal of Intelligent Material Systems and Structures* 23:15–23.

Allik, H., and T. J. R. Hughes. 1970. "Finite Element Method for Piezoelectric Vibration." *International Journal for Numerical Methods in Engineering* 2:151–157.

Becker, J., O. Fein, M. Maess, and L. Gaul. 2006. "Finite Element-Based Analysis of Shunted Piezoelectric Structures for Vibration Damping." *Computers & Structures* 84:2340–2350.

Cady, W. 1946. *Piezoelectricity*. New York: McGraw-Hill.

Collet, M., and K. Cunefare. 2008. "Modal Synthesis and Dynamical Condensation Methods for Accurate Piezoelectric Systems Impedance Computation." *Journal of Intelligent Material Systems and Structures* 19:1251–1269.

Dyke, K. V. 1928. "The Piezo-Electric Resonator and Its Equivalent Network." *Proceedings of the Institute of Radio Engineers* 16:742–764.

Elvin, N., and A. Elvin. 2009. "A General Equivalent Circuit Model for Piezoelectric Generators." *Journal of Intelligent Material Systems and Structures* 20:3–9.

Erturk, A., and D. Inman. 2008. "Issues in Mathematical Modeling of Piezoelectric Energy Harvesters." *Smart Materials and Structures* 17 (6), 065016.

Hagood, N. W., W. H. Chung, and A. von Flotow. 1990. "Modelling of Piezoelectric Actuator Dynamics for Active Structural Control." *Journal of Intelligent Material Systems and Structures* 1:327–354.

Hohl, A., Neubauer, M., Panning, L., & Wallaschek, J. 2009. "Modelling of Shunted Piezoceramic Actuators with Substructure Techniques and Application to a Bladed Disk Model." *Proceedings IEEE/ASME International Conference on Advanced Intelligent Mechatronics (AIM), Singapore, July,* 1088–1093.

Holland, R., and E. EerNisse. 1968. "Variational Evaluation of Admittances of Multielectroded Three-Dimensional Piezoelectric Structures." *IEEE Transactions on Sonics and Ultrasonics* 15:119 –131.

Ikeda, T. 1996. *Fundamentals of Piezoelectricity*. Oxford: Oxford University Press.

Kandare, G., and J. Wallaschek. 2002. "Derivation and Validation of a Mathematical Model for Traveling Wave Ultrasonic Motors." *Smart Materials and Structures* 11:565.

Kattenstroth, R., H. Harms, T. Lang, W. Wurpts, J. Twiefel, and J. Wallaschek. 2011. "Reibkraftreduktion mittels Ultraschallanregung in der Bodenbearbeitung." *Landtechnik* 66:10–13. (in German).

Król, R. 2011. *Eine Reduktionsmethode zur Ableitung elektromechanischer Ersatzmodelle für piezoelektrische Wandler unter Verwendung der Finite-Elemente-Methode (FEM)*, Ph.D. thesis, Universität Paderborn. (in German).

Lenk, A., R. G. Ballas, R. Werthschützky, and G. Pfeifer. 2011. *Electromechanical Systems in Microtechnology and Mechatronics*. Berlin: Springer.

Littmann, W., H. Storck, and J. Wallaschek. 2001. "Sliding Friction in the Presence of Ultrasonic Oscillations: Superposition of Longitudinal Oscillations." *Archive of Applied Mechanics, Springer* 71:549–554.

Mason, W. 1942. *Electromechanical Transducers and Wave Filters*. New York: D. van Nostrand Company.

Popov, E. P., and I. P. Paltov. 1960. *Approximate Methods for Analyzing Nonlinear Automatic Systems*, Fizmatgiz. (In Russian, translations available).

Porfiri, M., C. Maurini, and J. Pouget. 2007. "Identification of Electromechanical Modal Parameters of Linear Piezoelectric Structures." *Smart Materials and Structures* 16:323–331.

Richter, B., J. Twiefel, and J. Wallaschek. 2009. "Piezoelectric Equivalent Circuit Models." In *Energy Harvesting Technologies*, edited by Shashank Priya and Daniel J. Inman, 107–128. New York: Springer.

Roundy, S., and P. K. Wright. 2004. "A Piezoelectric Vibration Based Generator for Wireless Electronics." *Smart Materials and Structures* 13:1131–1142.

Sodano, H., G. Park, and D. Inman. 2004. "Estimation of Electric Charge Output for Piezoelectric Energy Harvesting." *Strain* 40:49–58.

Tiersten, H. 1969. *Linear Piezoelectric Plate Vibrations*. Plenum Press.

Tiersten, H. F. 2013. *Linear Piezoelectric Plate Vibrations: Elements of the Linear Theory of Piezoelectricity and the Vibrations Piezoelectric Plates*. New York: Springer (Reprint from 1. Ed.1969).

Tilmans, H. 1997. "Equivalent Circuit Representation of Electromechanical Transducers: II. Distributed-Parameter Systems." *Journal of Micromechanics and Microengineering* 7:285–309.

Twiefel, J., B. Richter, T. Sattel, and J. Wallaschek. 2008. "Power Output Estimation and Experimental Validation for Piezoelectric Energy Harvesting Systems." *Journal of Electroceramics* 20:203–208.

Wurpts, W., and J. Twiefel. 2013. "Analysis of Ultrasonic Vibro-Impact Systems with Equivalent Circuits and the Harmonic Balance Method." *Sensors and Actuators A: Physical* 200:114–122.